Applied Physics A (2018) 124:566
https://doi.org/10.1007/s00339-018-1967-9

Applied Physics A
Materials Science & Processing

Flexible solid-state supercapacitors based on carbon aerogel and some electrolyte polymer gels

T. Esawy[1] · M. Khairy[1,2] · A. Hany[1] · M. A. Mousa[1]

Received: 16 May 2018 / Accepted: 10 July 2018 / Published online: 26 July 2018

Abstract
Various energy devices with enhanced performance can be fabricated based on nanostructured carbons and conducting polymeric electrolytes. For instance, supercapacitors are attractive energy storage devices due to their high power density. In the present work, supercapacitors are fabricated using synthesized carbon aerogel as an active electrode in combination with different electrolytes. Electrolytes are important components in supercapacitors since their electrochemical properties directly influence the performance and the internal resistance of the capacitor. Aqueous electrolytes of KOH, H_2SO_4, H_3PO_4 and six different gel electrolytes PVA/KCL, PVA/H_3PO_4, PVA/H_2SO_4, PVA/KOH, and PVA/KOH–KCl–K_3[Fe(CN)$_6$] and PVA/KNO_3 are used for making flexible supercapacitors. The electrochemical properties of the different electrolytes are compared using cyclic voltammetry, galvanostatic charge/discharge curves and impedance spectroscopy. The capacitor containing PVA–KOH–KCl–K_3[Fe(CN)$_6$] electrolyte membrane with a weight ratio of 60:23:23:4 shows the highest specific capacitance of 520 F g^{-1} and a long cycling life with retention of 98.1% after 1000 cycles, also its specific capacitance increases with increasing the temperature from 25 to 70 °C.

1 Introduction

In the present time, a remarkable increase on maintainable storage technology occurred due to quick depletion of current energy sources (fossil fuel). Supercapacitor is one of energy storage devices with very high capacity that are able to store and deliver energy at relatively higher rates compared to other sustainable energy technologies such as batteries due to the mechanism of energy storage which includes a simple charge separation at the interface between the electrode and the electrolyte. Supercapacitor (SCs) stores energy with greater power density (10^3–10^6 W kg^{-1}) and lower energy density (1–10 W kg^{-1}) than batteries [1]. A supercapacitor comprises of two electrodes, an electrolyte, and a separator which insulates the two electrodes [1, 2]. Generally, there are two types of supercapacitors based on storage principle: (1) electrochemical double-layer capacitors (EDLCs) which store energy using the adsorption of both anions and cations at electrodes forming electric double layer and (2) pseudo-capacitors that store energy through fast surface reversible redox reactions between electrolyte and electro-active materials on the electrode surface [3, 4]. Supercapacitors were presented as a viable solution for energy storage challenges in high-power-demanding applications such as car starters, wind turbine energy storage, plug-in hybrid electric vehicles, and motor drives [5–7].

The type of electrode materials adjusts the performing of supercapacitors [4, 8]. Several transition metal oxides such as RuO_2, MnO_2, V_2O_5, Ferrites and so on and some conducting polymers, e.g. polyaniline and polypyrole are used as electrode materials in supercapacitors [9–11]. Moreover, porous carbon materials with different morphology and carbon nanotubes are the most-studied electrode materials for supercapacitors due to their low cost, high chemical stability, high conductivity, broad working temperature range and easy availability [12, 13].

The reported electrical capacitances for predominantly solid-state supercapacitors built using free-standing carbon such as graphene lie between 75 and 120 F g^{-1}, which is

Electronic supplementary material The online version of this article (https://doi.org/10.1007/s00339-018-1967-9) contains supplementary material, which is available to authorized users.

✉ M. Khairy
mohkhairy@fsc.bu.edu.eg

[1] Chemistry Department, Faculty of Science, Benha University, Benha, Egypt

[2] Chemistry Department, College of Science, Al-Imam Mohammad Ibn Saud lslamic University, Riyadh, Kingdom of Saudi Arabia

far less than the related theoretical value (550 F g^{-1}) [14] because of the restocking of graphene layers causing a decrease in the active surface area and slowing down the transport of the ions inside the active materials. To rise above this drawback, porous 3D carbon networks have been devised as active electrodes in electrochemical energy storage devices [15–19].

A great number of the recent researches on supercapacitors focused on liquid electrolytes [20] due to their high ionic conductivity with a short potential power supply range. However, their unfavorable effects such as liquid outflow, explosion risks, and corrosion [21] limited their applicability and allowed solid electrolytes to be presented as better candidates for reliable supercapacitors. Besides their easier handling, solid electrolytes have minimal internal corrosion, easier packaging, safer operation and lower environmental impacts [22].

Nowadays, great efforts have been committed to the improvement of all-solid-state supercapacitors [23–28]. Newly, Supercapacitor centered upon gel polymer electrolytes was searched by many instigators [29–33], especially flexible SCs because they can deliver significantly higher specific/volumetric energy density compared to conventional capacitors. Moreover, flexible solid-state supercapacitors are characteristically small in size, highly reliable, light weight and easy to handle [34, 35]. Among the polymers, PVA is more desirable because it is biodegradable, nontoxic, inexpensive and chemically stable. The PVA hydrogels also have high structural integrity and good mechanical properties [36, 37]. Polymeric gel-based electrolytes of PVAacid or alkali [38–41], polyethylene oxide (PEO)-alkali [42], potassium polyacrylate (PAAK)-salt or alkali [43, 44] have been reported. The use of biopolymer gel as chitosan in supercapacitor devices has been also registered [9, 45].

Symmetric supercapacitor consists of activated carbon as electrodes and PVA–KOH–$K_3[Fe(CN)_6]$ gel electrolyte was investigated and showed a good electrochemical performance with a specific capacitance of 431 F g^{-1}, energy and power densities values of 57.94 W kg^{-1} and 59.84 kW kg^{-1}, respectively [46]. Whereas, Ramasamy et al. reported a specific capacitance of 24 F g^{-1}, power of 0.52 kW kg^{-1}, and energy density of 18.7 W kg^{-1} for symmetric capacitor cell which consists of activated carbon electrode and a gel electrolyte of sodium salt–polyethylene oxide [47]. Gao et al. also reported an energy density of 32.7 W kg^{-1} for asymmetric capacitor cell, which consists of carbon nanotube–manganese oxide electrodes based on potassium polyacrylate gel [48].

The used electrolytes in the present work were previously characterized in an earlier published paper [49] from our group. The samples were investigated using XRD and FT-IR besides determining their surface area and pore sizes. Moreover, we have compared the ionic conductivity, transport number and mechanical properties of the electrolytes in the prior work [49]. The results obtained showed that the CA exhibits a significantly high surface area of 934 m^2 g^{-1} with a pore diameter ranging between 5.2 and 8.1 nm [49]. The synthesized PVA membranes doped by H_2SO_4, H_3PO_4, KOH, KCl and $K_3[Fe(CN)_6]$ had amorphous flexible structure that is easily bendable and exhibited high ionic conductivity in the range of 4.1×10^{-3}–7.0×10^{-2} with ionic transport number in the range of 0.97–0.99 [49]. On the other hand, the PVA–KOH–KCl–$K_3[Fe(CN)_6]$ solid polymer electrolyte with a weight ratio of 60:23:23:4 exhibited the highest room temperature ionic conductivity of 7×10^{-2} S cm^{-1} [49].

In the present work, we tested and reported the electrochemical properties of several flexible supercapacitors which consist of carbon aerogel (CA) as an active electrode material and different aqueous electrolytes (KOH, KCl, H_2SO_4, H_3PO_4) as well as several solid-state electrolytes based on PVA gel: (PVA–KOH), (PVA–KCl), (PVA–KOH–KCl), PVA–KOH–KCl–$K_3[Fe(CN)_6]$, (PVA–H_2SO_4) and (PVA–H_3PO_4). The electrical capacitance values are compared. And the effect of temperature on the capacitance value was examined at temperatures between 25 and 70 °C.

2 Experimental

2.1 Materials

Resorcinol ($C_6H_6O_2$) and methyl cellulose were purchased from El-Gamhouria Co., formaldehyde solution (34.5–38%) and polyvinyl alcohol (PVA) from El- Nasr pharmaceutical Co., potassium hydroxide (KOH) and KCl provided from Adwick, sodium carbonate (Na_2CO_3), phosphoric acid (H_3PO_4) and sulphuric acid (H_2SO_4) from Sigma-Aldrich. Deionized water was used in all preparation methods.

2.2 Preparation of carbon aerogel (CA)

Resorcinol–formaldehyde polymer precursor was synthesized by polycondensation of resorcinol with formaldehyde in an aqueous solution. First, an aqueous solution of sodium carbonate as a catalytic material was mixed with resorcinol (R) to accelerate its dehydrogenation. Formaldehyde (F) was then added slowly to the above-stirred solution to get 1:2 a molar ratio of ($R/F = 1/2$), and the weight % of reactants in solution was ~40%. The ratio of R: catalyst ratio was fixed at 1000. The resulting solution was then cured at 80 °C for 3 days in a vial to form a cylindrical shape. The water present in RF was exchanged with acetone at 55 °C for 24 h every 3 h. To eliminate water thoroughly from the pores of RF wet gel, complete drying was then performed at 55 °C for

24 h [49]. Finally, carbon aerogel was prepared by pyrolysis of resorcinol–formaldehyde at 800 °C for 3 h under nitrogen flow [50].

2.3 Preparation of carbon aerogel electrodes

Homogeneous slurry of CA, acetylene black and binder PVDF (poly vinylidene fluoride) in the weight ratio 85:7.5:7.5 was fully milled in an agate mortar and bound with ethanol at room temperature. The obtained slurry was coated onto stainless steel mesh and dried at 60 °C for 36 h to get the electrode.

2.4 Preparation of gel polymer electrolyte

Alkaline and acidic basic PVA polymer electrolyte membrane series were prepared. An amount of 0.02 mol of an individual or combined electrolytes of H_3PO_4, H_2SO_4, KOH, and KCl was inserted into PVA (1 g) in deionized water (10 ml) followed by stirring and heating.

2.4.1 Preparation of alkaline gel polymer electrolytes

Alkaline PVA gel polymer electrolytes were fabricated according to the following method. 0.02 mol KOH was added to 1 g PVA dissolved in 10 ml deionized water. The mixture was stirred and heated at 90 °C until appearance homogeneous viscous solution. The viscous solution was then transferred to glass Petri dishes and leaves overnight at room temperature to evaporate the excess water and get a thick PVA–KOH gel polymer. All the studied gel polymers with different compositions were prepared by the same above-mentioned method; where 0.01 mol KCl and 0.01 mol KOH and 1 g PVA were used to prepare PVA–KOH–KCl gel polymers. Two ternary PVA–KOH–K_3[Fe $(CN)_6$] gel polymers were also synthesized using 0.01 mol KCl, 0.01 mol KOH and 5×10^{-4} or 1×10^{-3} mol of $K_3[Fe(CN)_6]$. Moreover, quaternary gel polymer electrolyte of PVA–KOH–KCl–$K_3[Fe(CN)_6]$ was also made via 0.01 mol KOH, 0.01 mol KCl and 5×10^{-4} or 1×10^{-3} mol $K_3[Fe(CN)_6]$.

The gel polymers were denoted as PK, PKL, PKF2, PKF4, PKLF2, and PKLF4 for the electrolytes PVA–KOH, PVA–KOH–KCl, PVA–KOH–5×10^{-4} mol K_3[Fe $(CN)_6$], PVA–KOH–1×10^{-3} mol K_3[Fe $(CN)_6$], PVA–KOH–KCl–5×10^{-4} mol K_3[Fe $(CN)_6$] and PVA–KOH–KCl–1×10^{-3} mol K_3[Fe $(CN)_6$], respectively.

2.4.2 Preparation of acidic gel polymer electrolytes

Polymer electrolyte of PVA–H_3PO_4 was fabricated by the solvent molding method, namely 1 g of PVA was dispersed in 10 ml of double distilled water with stirring to get a clear solution. After that, 0.02 mol of H_3PO_4 was inserted into the solution with continuous stirring at room temperature for 24 h. The obtained viscous solution was thrown onto Teflon frames and dried in an oven at 60 °C for 24 h. The dried layers were stripped off from the casts and cut into 30 mm × 10 mm bands. This will be denoted as PP.

The PVA–H_2SO_4 polymer electrolyte was synthesized by the same method mentioned above but with replacing H_3PO_4 by H_2SO_4. The electrolyte obtained was denoted as PS.

2.5 Electrochemical measurements

The carbon aerogel (CA) electrode was arranged in the way: first, carbon aerogel, acetylene black and polytetrafluoroethylene in a mass ratio of 8:1:1 were blended and dissolved in 0.5 ml of *N*-methyl-2-pyrrolidone (NMP) to make smooth slurry. Next, the formed slurry was painted on a stainless steel net thickness 0.06 mm with an area of 1 cm^2 with a mass load of 1.8 mg cm^{-2}. Finally, drying is done at 60 °C for 24 h to get the CA electrode.

The electrochemical measurements were studied on a CHI660D electrochemical workstation. Cyclic voltammetry (CV), galvanostatic charge–discharge (CD), and impedance spectroscopy (EIS) were conducted using two-electrode technique. The devices were categorized in a two-terminal arrangement like in really commercially packed electrical capacitor designs. Figure 1S shows a schematic illustration of the fabricated supercapacitor.

CV measurements for the supercapacitor device CA/PKLF4/CA with highest capacitance were achieved at temperatures ranging between 25 and 70 °C. Before starting the measurements, the cell was kept in a furnace for 4 h until the desired temperature was reached.

All the solid-state supercapacitors consist of solid gel electrolyte sandwiched between two working electrodes. The concentrations of aqueous electrolytes used were: 6 M KOH, 1 M H_2SO_4, and 1 M H_3PO_4.

The capacity values were estimated from CV plots using the following equations [51, 52]:

$$C_{\text{cell}}(F) = \left(\int I\mathrm{d}v\right)/\Delta V \times \nu, \tag{1}$$

where C_{cell} is the capacitance of the cell, I is the charging/discharging current, ΔV is the potential window, and ν is the scanning rate.

The specific capacitance C_{sp} was computed from C_{cell} and active mass of the electrode (m_{a}) as follows:

$$C_{\text{sp}} = 2C_{\text{cell}}/m_{\text{a}}. \tag{2}$$

The specific supercapacitor cell capacitance (C, $F\ g^{-1}$) and electrode-specific capacitance (C_{sp}, $F\ g^{-1}$) were also calculated from charge/discharge (CD) curves as follows [53, 54]:

$$C = I_d \times \Delta t / \Delta V \times m_a, \quad (3)$$

$$C_{sp} = 4 \times C. \quad (4)$$

Energy density (E), equivalent series resistance (ESR) and power density (P) of the supercapacitor were evaluated by the following equations [55]:

$$E = \left[\left(C \times \left(\Delta V^2\right)\right)/2\right] \times (1000/3600), \quad (5)$$

$$\mathrm{ESR} = iR_{\mathrm{drop}}/\left(2 \times I_d\right), \quad (6)$$

$$P = (\Delta V)^2/\left(4 \times \mathrm{ESR} \times m_a\right), \quad (7)$$

where iR drop is the voltage drop between the first two points of the discharge plot, I_d (A) is the discharge current and ΔV is the working voltage window of the supercapacitor.

3 Results and discussion

3.1 Cyclic voltammetry

The electrochemical behavior of the investigated capacitors in each of aqueous and solid gel electrolytes capacitor was studied by cyclic voltammetry at 10 mV s^{-1} and room temperature using two-electrode methods. The cyclic voltammograms obtained are illustrated in Figs. 1, 2. The CV curves of all capacitors, except that containing H_2SO_4 or $K_3[Fe(CN)_6]$ do not display any redox peaks, which denotes that the charge-storage mechanism is grounded on the electrostatic or physical disconnection of charges [56]. The redox peaks observed for the solid electrolyte containing $K_3[Fe(CN)_6]$ is attributed to a formation of $[Fe(CN)_6]^{3-}$ or $[Fe(CN)_6]^{4-}$ in the charge route, and thus a reversible redox consequence happens. The redox course at the electrolyte|electrode interface as results of the following [46]:

$$\left[\mathrm{Fe(CN)_6}\right]^{3-} + \mathrm{e}^- \rightleftharpoons \left[\mathrm{Fe(CN)_6}\right]^{4-}. \quad (8)$$

The capacitance C_{cell} and specific capacitance C_{sp} of the cell were obtained by calculating the charge under the curves along the voltage applied as given by Eqs. (1) and (2). The results obtained are given in Table 1. The capacitance was found to decrease in the order:

PKLF4 > PKLF2 > PKF4 > PK(aq) > PP(aq) = PP > PKF2 > PK = PS (aq) > PS.

The higher capacitance values obtained for capacitance cells refer to the diffusion of ionic charges into the carbon aerogel with a large surface area, 934 m^2 g^{-1} [49].

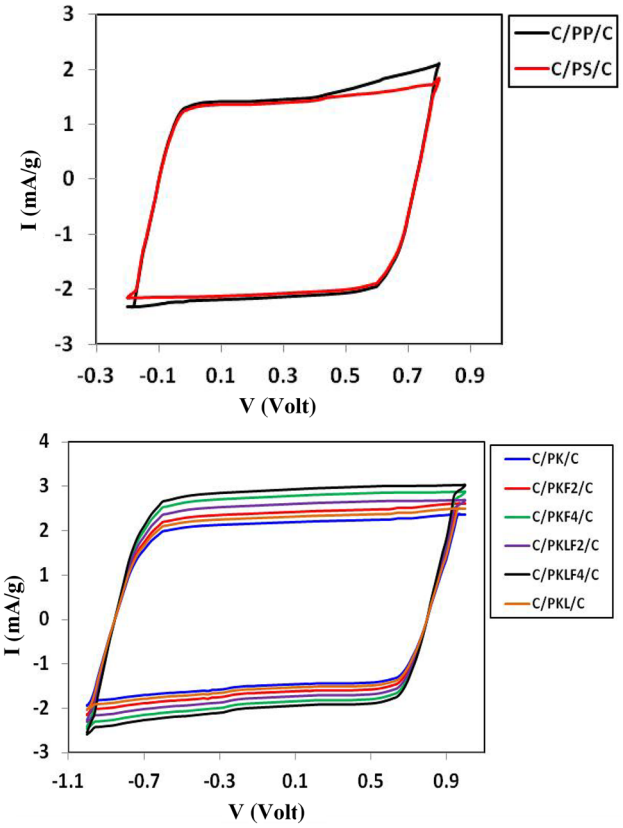

Fig. 1 The CV curves of C/PK/C, C/PS/C, C/PP/C, C/PKL/C, C/PKF2/C, C/PKF4/C, C/PKLF2/C and C/PKLF4/C supercapacitors at a scan rate of 10 mV s^{-1} in 6.0 M KOH

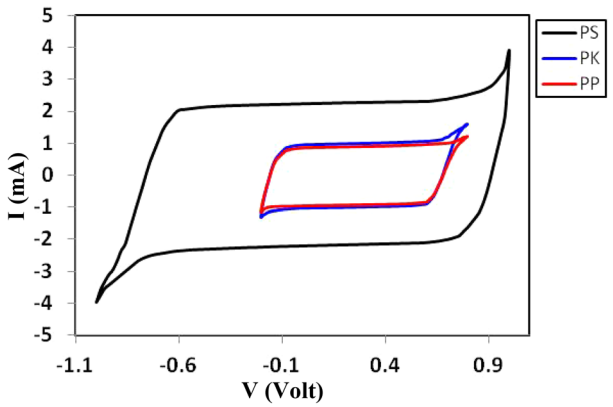

Fig. 2 The CV curves of PK, PS, and PP supercapacitors at a scan rate of 10 mV s^{-1} in 6.0 M KOH

The supercapacitor cell C/PKLF4/C exhibits the highest capacitance value in all the cells investigated. Therefore, CV was studied for this cell at various voltage scan rates and the results obtained are illustrated in Fig. 3. The shape of the voltammogram at various scan rates (1, 2, 5, 10, 20,

Table 1 Cell capacitance results obtained from CV at a scan rates 10 mV/s and charge–discharge (CD) at a current density 1 A g^{-1} for all the studied supercapacitors cells

Sample	*C* (CV) (F g^{-1})	*C* (CD) (F g^{-1})
CA/PKF2/CA	195	185
CA/PKF4/CA	218	202
CA/PKLF2/CA	219	208
CA/PKLF4/CA	260	240
CA/PP/CA	197	188
CA/PS/CA	166	170
CA/PK/CA	180	175
CA/PKL/CA	189	182
CA/aq KOH/CA	210	180
CA/aqH_3PO_4/CA	197	170
CA/aqH_2SO_4/CA	180	140

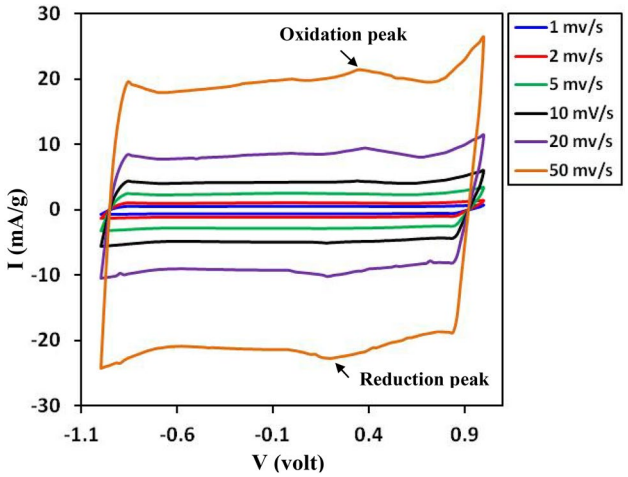

Fig. 3 The CV curves of C/PKLF4/C electrodes at scan rates of 1.0, 2, 5, 10, 20 and 50 mV s^{-1}

Table 2 Cell capacitance results obtained for C/PKLF4/C at various scan rates and charge–discharge (CD) at various current densities

Sample	Scan rate (mV s^{-1})	C_s (CV) (F g^{-1})	Current density (Ag^{-1})	C_s (charge/discharge) (F g^{-1})
C/PKLF4/C	1	305	2	226
	2	280	1	240
	5	270	0.5	250
	10	260	0.2	270
	20	240		
	50	221		

50 mV s^{-1}) is similar in nature, suggesting high charge transfer stability of the device even at high scan rates. The nearly rectangular shape of the CV curves indicates a near

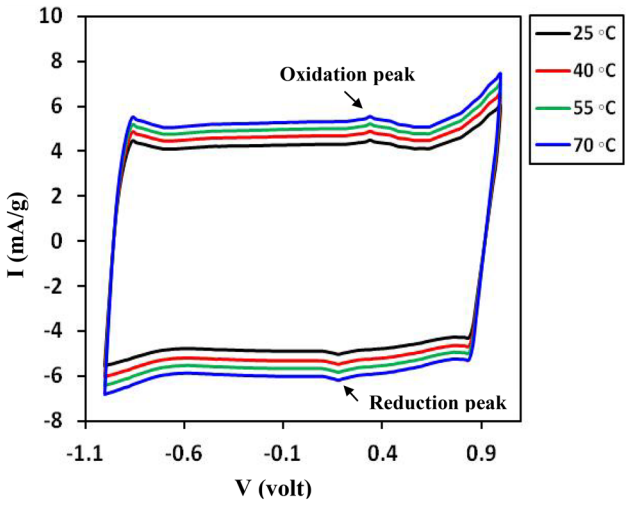

Fig. 4 The CV curves of C/PKLF4/C electrodes at different temperatures

ideal capacitive behavior [57]. The capacitance values are calculated and listed in Table 2.

The high capacitance obtained for the cell containing PVA–KOH –KCl–$K_3[Fe(CN)_6]$ gel electrolyte compared with the other cells can be attributed to each of the highest ionic conductivity value of PVA–KOH –KCl–$K_3[Fe(CN)_6]$ gel electrolyte comparable with the other membranes [49] and the contribution from the reversible redox reaction of $K_3[Fe(CN)_6]$ and its quick electron relay at the CA electrode–electrolyte membrane interface. The conductivity is originated from two ionic conductive mechanisms: the K^+, Cl^- and OH^- ions were transferred along the polymer molecular chain through the combination dissociation process between ions and the polar groups of the polymer and ion transfer tunnels as a result of the swelling structure. These ions accumulated at the CA electrode producing double-layer capacitance. The highest amorphous structure of PVA–KOH–KCl–$K_3[Fe(CN)_6]$ causes more ions to be transferred in the same time resulting from the developing of the motility of polymer chain segments, and finally the conductivity improved comparable with that other polymeric electrolyte system. Moreover, the pseudo-capacitance is produced in the membrane due to redox reaction occurring in the $[Fe(CN)_6]$ anion according to the mechanism illustrated in Eq. (8).

The effect of temperature on the charge-storage properties of the CA/PKLF/CA cell, which has the highest capacitance, were studied at temperature ranging between 25 and 70 °C using CV measurements at a scan rate of 10 mV s^{-1}. The obtained cyclic voltammograms showed similar shapes with a growth in the capacitive current with increasing the temperature, Fig. 4. This is attributed to increase the ionic conductivity of the membrane at elevated temperatures, where

the ions in the membrane move faster to reach the electrode surface compared to the situation at lower temperatures. The molecular alignment of polymeric chains with the increase in temperature might be also contribute to the increase in the specific capacitance.

3.2 Galvanostatic charge/discharge (CD) measurements

The CD technique is a dependable approach to assess the electrochemical capacitance of matters. Figure 5 demonstrates the CD—plots for the investigated supercapacitors at a current density of 1A g^{-1} at room temperature. Apparently, the discharge of the CA/PKLF4/CA cell exhibits its longer times than that the other supercapacitors. The capacitances of all the studied supercapacitor cells were evaluated according to Eq. 3, and the values obtained are listed in Table 1. The results obtained show that the specific capacitance of the supercapacitors increases in the sequence:

PKLF4 > PKLF2 > PKF4 > PP > PKF2 > PK (aq)>PK > PP(aq) ~ PS > PS (aq).

Inspection of Fig. 5 shows that the supercapacitors have iR_{drop} depend on the composition of the gel polymeric electrolyte. The ESR value is calculated from this voltage drop according to Eq. 6 for all the supercapacitors and listed in Table 3.

The equivalent series resistance is the summation of the major resistance of all materials present in the capacitor in addition to the contact resistance between them. The decrease in ESR might be due to: (a) enhancement in the ionic conductivity of the polymer electrolytes; and (b) the improved coincidence between the electrodes and the polymer electrolyte through charge transfer between the facilitators [58]. The obtained results show that the supercapacitor with CA/PKLF4/CA exhibits the smallest ESR value. This value is comparable with the results obtained by other researchers who observed ESR values for carbon electrodes ranging from 1.17 to 16.7 ohm for carbon electrodes derived from activated carbon powder [59, 60]. These literature ESR values obtained from EIS data are smaller than those obtained from the CD data. This tendency is also detected in the ESR results obtained here.

This is because the PKLF4 gel polymer exhibits the highest ionic conductivity in all the gel polymers studied [49].

More inspection of Fig. 5 demonstrates that the charge curves of the cell with PKF4, H_2SO_4 or H_3PO_4 are nearly straight and proportioned to their discharge complements, showing a significant of development by $K_3[Fe(CN)_6]$ and the other electrolytes on the electrochemical implementations of the supercapacitor. The increase in charge–discharge times of the cells containing $K_3[Fe(CN)_6]$ than that in the other cells might be attributed to the extraordinary influence of reversible redox course by $K_3[Fe(CN)_6]$, as mentioned above. Thus, the total capacitance of the electrochemical device is produced from the electrical double-layer capacitance obtained from the ions present on the surface of CA electrode and the pseudo-capacitance generated from $[Fe(CN)_6]^{3-}/[Fe(CN)_6]^{4-}$ reversible redox on the electrolyte|electrode interface.

The CD behaviors of the supercapacitor device of CA/PKLF4/CA, which has the highest capacitance value, were studied at different current densities of 0.2, 0.5, 1 and 2 A g^{-1} and the results obtained are shown in Fig. S2. The cell capacitances (C) at these current densities are calculated according to Eq. 3 and listed in Table 2. It is obvious that the device capacitance gradually decreases as the current density increases. This outcome points to the outstanding electrochemical properties of the cell with PKLF4 electrolyte under high current density, and it exhibits

Table 3 Characteristic parameters for supercapacitors CA/gel electrolyte/CA

Sample	C (F g^{-1})	ESR (Ω)	E (W kg^{-1})	P (KW kg^{-1})
PK	175	20.7	15.6	31.2
PKL	189	11.2	21.3	44.9
PKF2	185	5.25	23.2	54.2
PKF4	202	4.65	25.3	67.8
PKLF2	208	3.66	23.4	74.2
PKLF4	240	3.98	30.1	71.5

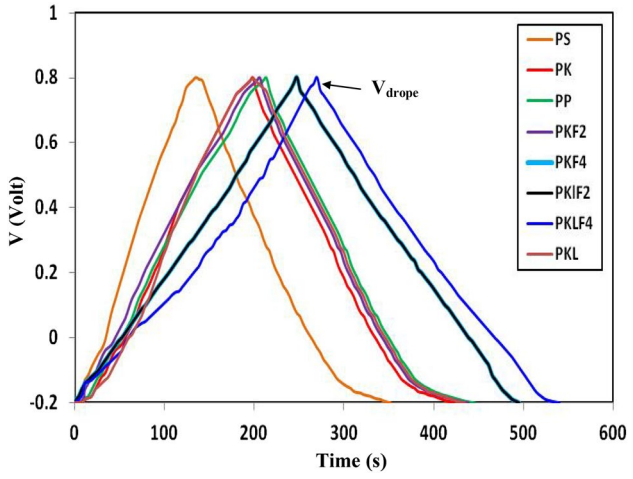

Fig. 5 The galvanostatic charge–discharge curves of PK, PS, PP, PKL, PKF, PKLF2 and PKLF4 electrodes during current density of 1.0 A g^{-1} in 6.0 M KOH electrolytes

improved rate ability than the other supercapacitors without $[Fe(CN)_6]^{3-}/[Fe(CN)_6]^{4-}$.

For all supercapacitor cells, the energy (E) and power (P) densities were computed from CD process at numerous current densities using Eqs. (5) and (7), and are listed in Table 3.

3.3 Electrochemical impedance spectroscopy (EIS)

Electrochemical impedance spectroscopy (EIS) is used to get information about the chemical and physical progressions taking place on the electrode surface, the different frequency reply of supercapacitors and the capacitive trends taking place in the electrodes. The Nyquist plots of CA in various aqueous electrolytes are shown in Fig. 6, which shows semicircle represents the dominant resistive nature of a porous electrode. The charge transfer (CT) process at the electrode–electrolyte interface is described by the discrete section represented by a semicircle at higher frequencies, whereas the straight line inclined at an angle of ~ 90° to the real axis identifies the diffusion-controlled electrode kinetics at low-frequency zone. The charge transfer process (CT) at the CA electrode–electrolyte interface is explained by the distinct region represented by a semicircle at higher frequencies [60, 61]. The CT values are found to be 0.3, 0.91 and 1.01 Ω for KOH, H_3PO_4 and H_2SO_4 electrolytes, respectively.

The impedance spectra of CA/gel electrolyte/CA supercapacitor devices are shown in Fig. 7. The plots are similar to that found in aqueous electrolyte. The results obtained are summarized and listed in Table 3. From which it is noted that the diameter of the semi-circle representing the charge transfer resistance R_{ct} is decreasing by the addition of $K_3[Fe(CN)_6]$ to the PVA/KOH electrolyte gel.

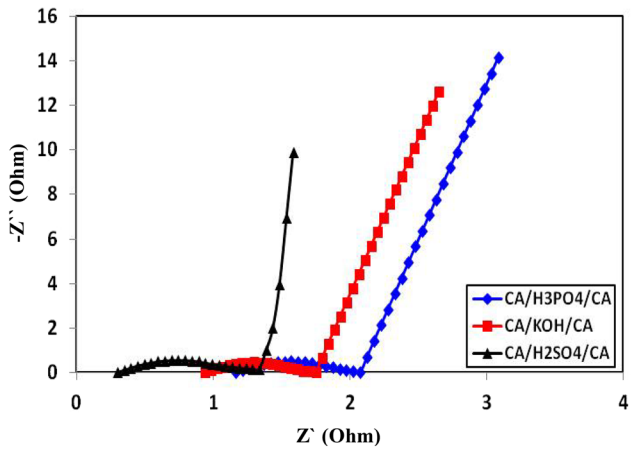

Fig. 6 Impedance spectra of CA/KOH/CA, CA/H_2SO_4/CA, and CA/H_3PO_4/CA supercapacitors

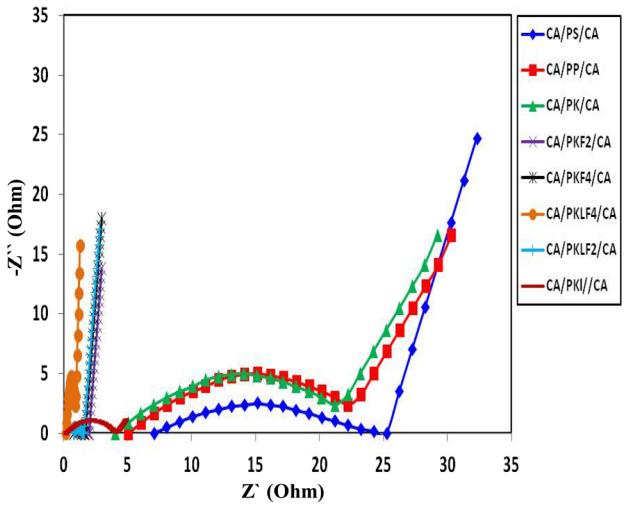

Fig. 7 Impedance spectra of CA/PK/CA, CA/PS/CA, CA/PP/CA, CA/PKL/CA, CA/PKF2/CA, CA/PKF4/CA, CA/PKLF2/CA and CA/PKLF4/CA supercapacitors

Electrochemical impedance spectroscopy also provides further information including the time constant for charging and discharging of the supercapacitor device. The imaginary part reaches a maximum at a particular frequency f_o which is used to determine the time constant $\tau_o = 1/f_o$. The relaxation times obtained for the different devices are listed in Table 4. The cell containing $K_3[Fe(CN)_6]$ electrolyte exhibits much lower time constant value than that of other devices. These results are supported by the results obtained from CV and GC data that the $K_3[Fe(CN)_6]$ can charge and discharge over much shorter times and is potentially a good candidate for high-frequency applications.

3.4 Life cycle analysis

Long cycle life of supercapacitor is a very important parameter when it comes to practical applications. Therefore, the cycling durability of the CA/PKLF4/CA capacitor device (highest C value) was tested by charge/discharge

Table 4 R_{ct} and the time constants of CA/gel electrolyte/CA devices

Sample	R_{ct} (Ω)	τ_o (s) × 10^2
CA/PKLF4/CA	0.76	1.5
CA/PKLF2/CA	0.84	1.0
CA/PKF4/CA	0.87	2.1
CA/PKF2/CA	0.90	2.5
CA/PKL/CA	3.95	4.4
CA/PK/CA	17.03	5.1
CA/PS/CA	18.23	6.5
CA/PP/CA	17.16	9.2

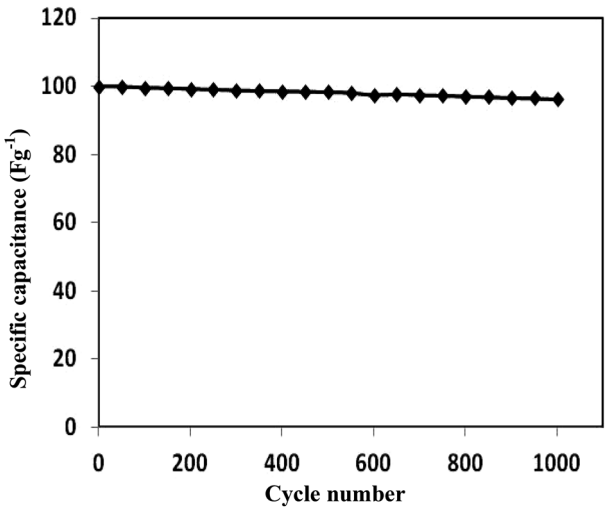

Fig. 8 The galvanostatic charge–discharge curve in the potential range from − 1.1 to 0.9 for 1000 cycles for PKLF4 electrodes

(CD) cycling at a current density of 1 A g^{-1} and the results obtained are given in Fig. 8. It is seen that the supercapacitors have excellent cycle stability with retention of 96.4%, and of their first electrode-specific capacitances after 1000 cycles. This may be attributed to the good contact between the polymer electrolyte and the carbon aerogel electrode. Consequently, contact incoherence between the CA electrode and the polymeric electrolyte does not happen during CD process.

Table 5 shows a comparison between the electrochemical properties of our CA/PKLF4/CA supercapacitor device and similar devices reported in the literatures [62–70], at room temperature. It can be seen that our capacitor exhibits high C_{sp}, E_m and P_m values compared with the most reported capacitors.

4 Conclusions

Carbon aerogel (CA) was synthesized by pyrolysis of resorcinol–formaldehyde and used as an electrode with PVA-based gel polymer electrolyte for fabricating supercapacitors. PVA films doped with different electrolytes (H_2SO_4, H_3PO_4, KOH, KCl, $K_3[Fe(CN)_6]$) were successfully prepared using solution casting technique. The supercapacitor was constructed by one PVA-based electrolyte inserted between two CA electrodes. With the favorable impact of $K_3[Fe(CN)_6]$ redox reaction and its rapid electron exchange at the electrode–electrolyte interface, the prepared capacitor device CA/PVA–KOH–KCl–$K_3[Fe(CN)_6]$/CA showed excellent performance. It had large electrode-specific capacitance (520 F g^{-1}), maximum energy density (30.1 W kg^{-1}), maximum power density (71.5 kW h^{-1}) and high cycle life that keeps 96.4% of the original capacitance values after 1000 cycles. The capacitor device was stable in the temperature range of 25–70 °C and its capacitance increased with increasing temperature. The results elucidate the potential of using $K_3[Fe(CN)_6]$ in improving solid-state supercapacitor performance ionic conductivity and pseudo-capacitance. This study provides a simple and straightforwardly scalable approach to fabricate stretchy and lightweight supercapacitors.

Table 5 Comparison of electrochemical performance of the studied CA/PKLF4/CA supercapacitor with similar capacitors in the literature

Assembled supercapacitor	C (F g^{-1})	E_m (W kg^{-1})	P_m (kw h^{-1})	References
AC/PVA–KOH–$K_3[Fe(CN)_6]$/AC	215.5	57.9	59.8	[46]
AC/Na salt–PEO/AC	24	18.7	0.52	[47]
PC/Na_2SO_4/PVA/PC	150.8	17.37	13.5	[62]
AC/KOH(aq)/AC	210	16.9	0.2	[63]
N-dopedPC/PVA–KOH/N-dopedPC	306	–	–	[64]
rGO/SWNTs/PVAH_3PO_4/rGO/SWNTs	52.5	–	–	[65]
C/Nafion/C	123	–	–	[66]
G-dopedC/ion gel/C-doped C	190	76	–	[67]
PAM-polyacrylamide–KOH gel/AC	196	28.6	10	[68]
AC/SC–PVA–0.25M H_2SO_4/AC	64	–	–	[69]
AC/Nafion ionomer/AC	114	–	–	[70]
CA/PKLF4/CA	240	30.1	71.5	Present work

C cell capacitance, E_m maximum energy density, P_m maximum power density, *AC* activated carbon, *PC* polycarbonate, *G* graphene, *rGO* reduced graphene oxide, *SWNT* single wall nanotube, *PEO* polyethylene oxide, *SC* sulphated cellulose, *Na-salt* sodium bis(trifluoromethanesulfonyl)imide (NaTFSI)

References

1. M.D. Stoller, S. Park, Y. Zhu, J. An, R.S. Rouf, Graphene-based ultracapacitors. Nano Lett **8**, 3498–3502 (2008)
2. H.P. Wu, D.W. He, Y.S. Wang, M. Fu, Z.L. Liu, J.G. Wang, H.T. Wang, Graphene as the electrode material in supercapacitors, 8th international vacuum electron sources conference and nanocarbon, IEEE, pp 465–466 (2010)
3. G. Xiong, C. Meng, R.G. Reifenberger, P.P. Irazoqui, T.S. Fisher, A review of graphene-based electrochemical microsupercapacitors. Electroanal 26, **30**–**51** (2014)
4. Z.S. Iro, C. Subramani, S.S. Dash, A brief review on electrode materials for supercapacitor. Int. J. Electrochem. Sci. **11**, 10628–10643 (2016)
5. P. Simon, Y. Gogotsi, Materials for electrochemical capacitors. Nat. Mater. **7**, 845–854 (2008)
6. R.F. Service, New 'supercapacitor' promises to pack more electrical punch. Sci. Mater. Sci. 313, 902 (2006)
7. A. Hammar, P. Venet, R. Lallemand, G. Coquery, G. Rojat, Study of accelerated aging of supercapacitors for transport applications. IEEE Trans. Ind. Electron. **57**, 3972–3979 (2010)
8. Z. Yu, L. Tetard, L. Zhai, J. Thomas, Supercapacitor electrode materials: nanostructures from 0 to 3 dimensions. Energy Environ. Sci. **8**, 702–730 (2015)
9. R. Ramkumar, M.M. Sundaram, Electrochemical synthesis of polyaniline cross-linked $NiMoO_4$ nanofibre dendrites for energy storage devices. New J. Chem. **40**, 7456–7464 (2016)
10. L. Bao, J. Zang, X. Li, Flexible Zn_2SnO_4/MnO_2 core/shell nanocable-carbon microfiber hybrid composites for high-performance supercapacitor electrodes. Nano Lett. **11**, 1215–1220 (2011)
11. X. Liu, G. Du, J. Zhu, Z. Zeng, X. Zhu, $NiO/LaNiO_3$ film electrode with binder-free for high performance supercapacitor. Appl. Surf. Sci. **384**, 92–98 (2016)
12. D. Hulicova-Jurcakova, M. Kodama, S. Shiraishi, H. Hatori, Z.H. Zhu, G.Q. Lu, Nitrogen-enriched nonporous carbon electrodes with extraordinary supercapacitance. Adv. Funct. Mater. **19**, 1800–1809 (2009)
13. K.-X. Sheng, Y.-X. Xu, C. Li, G.-Q. Shi, High-performance self-assembled graphene hydrogels prepared by chemical reduction of graphene oxide. New Carbon. Mater. **26**, 9–15 (2011)
14. R.S. Dey, H.A. Hjuler, Q. Chi, Approaching the theoretical capacitance of graphene through copper foam integrated three-dimensional graphene networks. J. Mater. Chem. A **3**, 6324–6329 (2015)
15. Y. Xu, K. Sheng, C. Li, G. Shi, Self-assembled graphene hydrogel via a one-step hydrothermal process. ACS Nano **4**, 4324–4330 (2010)
16. L. Zhang, G. Shi, Preparation of highly conductive graphene hydrogels for fabricating supercapacitors with high rate capability. J. Phys. Chem. C **115**, 17206–17212 (2011)
17. J. Chen, K. Sheng, P. Luo, C. Li, G. Shi, Graphene hydrogels deposited in nickel foams for high-rate electrochemical capacitors. Adv. Mater. **24**, 4569–4573 (2012)
18. X. Zhang, Z. Sui, B. Xu, S. Yue, Y. Luo, W. Zhan, B. Liu, Mechanically strong and highly conductive graphene aerogel and its use as electrodes for electrochemical power sources. J. Mater. Chem. **21**, 6494–6497 (2011)
19. Z.S. Wu, A. Winter, L. Chen, Y. Sun, A. Turchanin, X. Feng, K. M¨ullen, Three-dimensional nitrogen and boron co-doped graphene for high-performance all-solid-state supercapacitors. Adv. Mater. **24**, 5130–5135 (2012)
20. B.E. Conway, *Electrochemical supercapacitors scientific fundamentals and technological applications* (Plenum Press, New York, 1999)
21. D. Kalpana, N.G. Renganathan, S. Pitchumani, A new class of alkaline polymer gel electrolyte for carbon aerogel supercapacitors. J. Power Sources **157**, 621–623 (2006)
22. X. Liu, T. Momma, T. Osaka, All-solid state electric double layer capacitor using polymer electrolyte and isotropic high density graphite electrodes. Chem. Lett. **25**, 625–626 (1996)
23. C. Huang, J. Zhang, N.P. Young, H.J. Snaith, P.S. Grant, Solid-state supercapacitors with rationally designed heterogeneous electrodes fabricated by large area spray processing for wearable energy storage applications. Sci. Rep. 6, 25684 (1–15) (2016)
24. M.G. Hosseini, E. Shahryar, Fabrication of novel solid-state supercapacitor using a Nafion polymer membrane with graphene oxide/multiwalled carbon nanotube/polyaniline. J. Solid State Electrochem. **21**, 2833–2848 (2017)
25. M. Genovese, H. Wu, A. Virya, J. Li, P. Shen, K. Lian, Ultrathin all-solid-state supercapacitor devices based on chitosan activated carbon electrodes and polymer electrolytes. Electrochim. Acta **273**, 392–401 (2018)
26. Y.L. Li, P.C. Li, B.J. Li, M.K. Gao, F.Y. Zhao, L. Shao, J.F. Chen, L.H. Li, All-solid-state flexible supercapacitors based on screen-printed graphene electrodes. Int. J. Electrochem. Sci. **12**, 10567–10576 (2017)
27. C. Yanga, L. Zhanga, N. Hua, Z. Yanga, H. Wei, Y. Wang, Y. Zhanga, High-performance flexible all-solid-state supercapacitors based on densely-packed graphene/polypyrrole nanoparticle papers. Appl. Surface Sci. **387**, 666–673 (2016)
28. Z. Li, Z. Zhou, G. Yun, K. Shi, X. Lv, B. Yang, High-performance solid-state supercapacitors based on graphene-ZnO hybrid nanocomposites. Nanoscale Res. Lett. **8:473**, 1–9 (2013)
29. N.A. Choudhury, S. Sampath, A.K. Shukla, Gelatin hydrogel electrolytes and their application to electrochemical supercapacitors. J. Electrochem. Soc. **155**, A74–A81 (2008)
30. M. Rosi, F. Iskandar, M. Abdullah, Khairurrijal, hydrogel-polymer electrolytes based on polyvinyl alcohol and hydroxyethylcellulose for supercapacitor applications. Int. J. Electrochem. Sci. **9**, 4251–4256 (2014)
31. Y.N. Sudhakar, M. Selvakumar, D.K. Bhat, Lithium salts doped biodegradable gel polymer electrolytes for supercapacitor application. J. Mater. Environ. Sci. **6**, 1218–1227 (2015)
32. P. Sivakumar, M. Gunasekaran, M. Sasikumar, A. Jagadeesan, PVDF-HFP based porous polymer electrolyte for lithium battery applications. Inter. J. Sci. Res. **2**, 2319–7064 (2013)
33. P.F.R. Ortega, J.P. C.Trigueiro, G.G. Silva, R.L. Lavall, Improving supercapacitor capacitance by using a novel gel nanocomposite polymer electrolyte based on nanostructured SiO_2, PVDF and imidazolium ionic liquid. Electrochim. Acta **188**, 809–817 (2016)
34. L. Nègre, B. Daffos, V. Turq, P.-L. Taberna, P. Simon, Ionogel-based solid-state supercapacitor operating over a wide range of temperature. Electrochim. Acta **206**, 490–495 (2016)
35. X. Lu, M. Yu, G. Wang, T. Zhai, S. Xie, Y. Ling, Y. Tong, Y. Li, $H\text{-}TiO_2@MnO_2//H\text{-}TiO_2$ @C Core–Shell nanowires for high performance and flexible asymmetric supercapacitors. Adv. Mater. **25**, 267–272 (2013)
36. Hu Ruofei, J. Zhao, R. Jiang, J. Zheng, Preparation of high strain polyaniline/polyvinyl alcohol composite and its applications in stretchable supercapacitor. J. Mater. Sci. Mater. Electron. **28**, 14568–14574 (2017)
37. T.S. Gaaz, A.B. Sulong, M.N. Akhtar, A.A.H. Kadhum, A.B. Mohamad, A.A. Al-Amiery, Properties and applications of polyvinyl alcohol, halloysite nanotubes and their nanocomposites. Molecules **20**, 22833–22847 (2015)
38. C.Z. Meng, C.H. Liu, L.Z. Chen, C.H. Hu, S.S. Fan, Highly flexible and all-solid-state paperlike polymer supercapacitors. Nano Lett. **10**, 4025–4031 (2010)
39. L.Y. Yuan, X.H. Lu, X. Xiao, T. Zhai, J.J. Dai, F.C. Zhang, B. Hu, X. Wang, L. Gong, J. Chen, C.G. Hu, Y.X. Tong, J. Zhou, Z.L. Wang, Flexible solid-state supercapacitors based on carbon nanoparticles/MnO_2 nanorods hybrid structure. ACS Nano **6**, 656–661 (2012)

40. B.G. Choi, J. Hong, W.H. Hong, P.T. Hammond, H. Park, Facilitated ion transport in all-solid-state flexible supercapacitors. ACS Nano **5**, 7205–7213 (2011)
41. F.H. Meng, Y. Ding, Sub-micrometer-thick all-solid-state supercapacitors with high power and energy densities. Adv. Mater. **23**, 4098–4102 (2011)
42. A. Lewandowski, M. Zajder, E. Frackowiak, F. Beguin, Supercapacitor based on activated carbon and polyethylene oxide–KOH–H_2O polymer electrolyte. Electrochim. Acta **46**, 2777–2780 (2001)
43. H.-S. Nam, N.-L. Wu, K.-T. Lee, K.M. Kim, C.G. Yeom, L.R. Hepowit, J.M. Ko, J.-D. Kim, Electrochemical capacitances of a nanowire-structured MnO_2 in polyacrylate-based gel electrolytes. J. Electrochem. Soc. **159**, A899–A903 (2012)
44. K.-T. Lee, N.-L. Wu, Manganese oxide electrochemical capacitor with potassium poly(acrylate) hydrogel electrolyte. J. Power Sources **179**, 430–434 (2008)
45. K. ZinHtut, M. Kim, E. Lee, G. Lee, S.H. Baeck, S.E. Shim, Biodegradable polymer-modified graphene/ polyaniline electrodes for supercapacitors. Synth. Metals **227**, 61–67 (2017)
46. G. Ma, J. Li, K. Sun, H. Peng, J. Mu, Z. Lei, High performance solid-state supercapacitor with PVA–KOH–$K_3[Fe(CN)_6]$ gel polymer as electrolyte and separator. J. Power Sources **256**, 281–287 (2014)
47. C. Ramasamy, J. Palma del vel, M. Anderson, An activated carbon supercapacitor analysis by using a gel electrolyte of sodium salt-polyethylene oxide in an organic mixture solvent. J. Solid State Electrochem. **18**, 2217–2223 (2014)
48. H. Gao, F. Xiao, C.B. Ching, H. Duan, Flexible all-solid-state asymmetric supercapacitors based on free-standing carbon nanotube/graphene and Mn_3O_4 nanoparticle/graphene paper electrodes. ACS Appl. Mater. Interfaces **4**, 7020–7026 (2012)
49. A. Hany, M.A. Mousa, T. El-Essawy, Studies on AC electrical conductivity, dielectric properties and ion transport in PVA polymeric electrolytes. J. Basic Environ. Sci. **4**, 298–304 (2017)
50. L. Lei, Z. Fu, Y. Yi, X. Huang, H. Tu, Ch Wang, Preparation and characterization of RF aerogel on UV irradiation method. J. Sol Gel. Sci. Technol. **72**, 553–558 (2014)
51. B.E. Conway, *Electrochemical supercapacitors: scientific fundamentals and technological applications* (Kluwer Academic/ Plenum Publishers, New York, 1999)
52. L. Huang, D. Chen, Y. Ding, S. Feng, Z.L. Wang, M. Liu, Nickel–cobalt hydroxide nanosheets coated on $NiCo_2O_4$ nanowires grown on carbon fiber paper for high-performance pseudocapacitors. Nano Lett. **13**, 3135–3139 (2013)
53. L.Q. Mai, A. Minhas-Khan, X. Tian, K.M. Hercule, Y.L. Zhao, X. Lin, X. Xu, Synergistic interaction between redox-active electrolyte and binder-free functionalized carbon for ultrahigh supercapacitor performance. Nat. Commun. **4**, 2923 (2013)
54. R. Vellacheri, A. Al-Haddad, H. Zhao, W. Wang, C. Wang, Y. Lein, High performance supercapacitor for efficient energy storage under extreme environmental temperatures. Nano Energy **8**, 231–237 (2014)
55. R. Vellacheri, A. Al-Haddad, H. Zhao, W. Wang, C. Wang, Y. Lei, High performance supercapacitor for efficient energy storage under extreme environmental temperatures. Nano Energy **8**, 231–237 (2014)
56. B.E. Conway, W.G. Pell, Double-layer and pseudocapacitance types of electrochemical capacitors and their applications to the development of hybrid devices. J. Solid State Electrochem. **7**, 637–644 (2003)
57. M.L. Verma, M. Minakshi, N.K. Singh, Structural and electrochemical properties of nanocomposite polymer electrolyte for electrochemical devices. Ind. Eng. Chem. Res. **53**, 14993–15001 (2014)
58. A.A. Łatoszyńska, G.Z. Żukowska, I.A. Rutkowska, P.-L. Taberna, P. Simon, P.J. Kulesza, W. Wieczorek, Non-aqueous gel polymer electrolyte with phosphoric acid ester and its application for quasi solid-state supercapacitors. J. Power Sources **274**, 1147–1154 (2015)
59. J.B. Wagner, C. Wagner, Electrical conductivity measurements on cuprous halides. J. Chem. Phys. **26**, 1597–1601 (1957)
60. S. Bindu, M.S. Suresh, Measurement of bulk resistance of conducting polymer films in presence of rectifying contacts. Inter. J. Sci. Res. **4**(8), 1–6 (2014). **ISSN 2250-3153**
61. L. Lai, H. Yang, L. Wang, B.K. Teh, J. Zhong, H. Chou, L. Chen, W. Chen, Z. Shen, R.S. Ruoff, J. Lin, Preparation of supercapacitor electrodes through selection of graphene surface functionalities. ACS Nano **6**, 5941–5951 (2012)
62. F. Yu, T. Wang, Z. Wen, H. Wang, High performance all-solid-state symmetric supercapacitor based on porous carbon made from a metal-organic framework compound. J. Power Source **364**, 9–15 (2017)
63. X. Sun, X. Zhang, H. Zhang, D. Zhang, Y. Ma, A comparative study of activated carbon-based symmetric supercapacitors in Li_2SO_4 and KOH aqueous electrolytes. J. Solid State Electrochem. **16**, 2597–2603 (2012)
64. K. Wang, M. Xu, Y. Gu, Z. Gu, Q.H. Fan, Symmetric supercapacitors using urea-modified lignin derived N-doped porous carbon as electrode materials in liquid and solid electrolytes. J. Power Source **332**, 180–186 (2016)
65. H.T. Jeong, Y.R. Kim, B.C. Kim, Flexible polycaprolactone (PCL) supercapacitor based on reduced graphene oxide (rGO)/single-wall carbon nanotubes (SWNTs) composite electrodes. J. Alloy Compds. **727**, 721–727 (2017)
66. P. Staiti, F. Lufrano, Nafion® and Fumapem® polymer electrolytes for the development of advanced solid-state supercapacitors. Electrochim. Acta **206**, 432–439 (2016)
67. X. Yang, L. Zhang, F. Zhang, T. Zhang, Y. Huang, Y. Chen, A high-performance all-solid-state supercapacitor with graphene-doped carbon material electrodes and a graphene oxide-doped ion gel electrolyte. Carbon **72**, 381–386 (2014)
68. D. Wang, L. Yu, B. He, L. Wang, A high-performance carbon–carbon(C/C) quasi-solid-state supercapacitor with conducting gel electrolyte. Int. J. Electrochem. Sci. **13**, 2530–2543 (2018)
69. B.S. Lalia, M. Alkaabi, R. Hashaikeh, Sulfated cellulose/polyvinyl alcohol composites as proton conducting electrolyte for capacitors. Energy Proc. **75**, 1869–1874 (2015)
70. P. Staitiz, F. Lufrano, Design, fabrication, and evaluation of a 1.5 F and 5 V prototype of solid-state electrochemical supercapacitor. J. Electrochem. Soc. **152**, A617–A621 (2005)